IEEE Photonics Journal
An IEEE Photonics Society Publication

Open Access

Digital Compensation of Relative Phase Noise for DSCM Based Coherent Transmission System Using Forward Pumped Distributed Raman Amplification

Volume 11, Number 1, February 2019

Govind Vedala, *Student Member, IEEE*
Youichi Akasaka, *Senior Member, IEEE*
Tadashi Ikeuchi, *Member, IEEE*
Rongqing Hui, *Senior Member, IEEE*

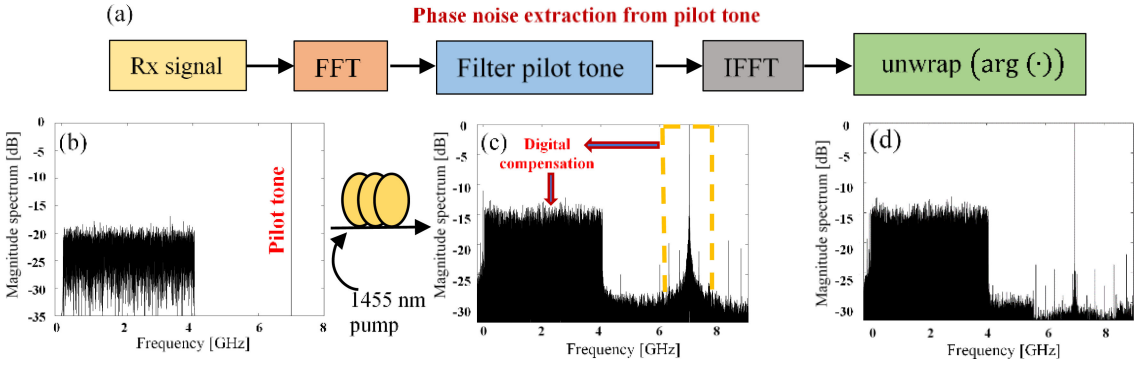

DOI: 10.1109/JPHOT.2018.2886462
1943-0655 © 2018 IEEE

Digital Compensation of Relative Phase Noise for DSCM Based Coherent Transmission System Using Forward Pumped Distributed Raman Amplification

Govind Vedala,[1] ***Student Member, IEEE*,**
Youichi Akasaka,[2] ***Senior Member, IEEE*,**
Tadashi Ikeuchi,[2] ***Member, IEEE*,**
and Rongqing Hui,[1] ***Senior Member, IEEE***

[1]Department of Electrical Engineering and Computer Science, University of Kansas, Lawrence, KS 66045 USA
[2]Fujitsu Laboratories of America, Inc., Richardson, TX 75082 USA

DOI:10.1109/JPHOT.2018.2886462

Manuscript received November 8, 2018; revised December 6, 2018; accepted December 8, 2018. Date of publication December 12, 2018; date of current version January 3, 2019. This work was supported in part by US National Science Foundation under Grant 1409853. Corresponding author: Govind Vedala (e-mail: govind.vedala@ku.edu).

Abstract: We experimentally demonstrate pilot aided compensation of relative phase noise (RPN) in a distributed Raman amplified coherent fiber optic system with forward pumping. This technique effectively eliminates the error floor that arises when conventional phase noise compensation algorithms track RPN, especially in the context of higher order modulation formats and low baud rate signals. Extrapolating the experimental results, we also demonstrate through measurement and simulation, the effectiveness of pilot aided RPN compensation in a 25 Gbaud, 16-QAM modulated digital-subcarrier system with 2.5 Gbaud and 5 Gbaud subcarriers.

Index Terms: Forward pumping, distributed Raman amplifier, Nyquist subcarrier, DSCM, relative phase noise, DSP.

1. Introduction

To enable high capacity data transmission, signaling at high baud rates with higher cardinality modulation formats (>16-QAM) is indispensable [1], [2]. Given the limited bandwidth (∼35 nm) supported by the C-band, extending the transmission into the L-band window proved imperative to transport ever increasing data traffic stemming from modern applications and services especially over long haul terrestrial and submarine links. The most popular amplification technologies for C+L band systems include lumped EDFAs, Distributed Raman Amplifiers (DRA) and hybrid Raman/EDFAs. Most of the experimental trials in laboratories reporting high capacity transmission made use of either all lumped or hybrid Raman/EDFAs [3], [4]. It is important to consider the fact that amplifier gain is always accompanied by ASE noise, which could compromise the reach that the modulated symbols are destined for. DRA offers enhanced OSNRs, low equivalent noise figures and wide gain bandwidth, but comes at the cost of high power pump modules, along with the impairments they cause on the information signal when transmitted through the same

fiber [5], [6]. The use of appropriate amplification scheme is indeed an important system design aspect involving performance benefits and economics. There are two important scenarios, where use of DRAs are mandatory to get to the desired reach, namely, multi-span systems with some spans extending to longer distances than the others, and unrepeated transmission systems. Fiber links deployed in remote forest areas and between islands are some examples where span lengths go beyond 200 km, without any inline amplification. Target reach for the above mentioned scenarios is achieved using both forward and backward pumped DRA, together with remote optically pumped amplification (ROPA) by minimizing the signal power variation along the fiber. The pump modules in DRAs supporting such long fiber spans offer high powers in the order of 1$\sim$2 W often accompanied with high relative intensity noise (RIN), on the level of $-100\sim-110$ dB/Hz [7], [8].

When propagating in the fiber along with the information signal, the RIN of the pump can be translated not only into the RIN but also the phase noise of the signal through cross-gain modulation (XGM) and cross-phase modulation (XPM). The latter is often referred to as RIN induced Relative Phase Noise (RPN) [9], [10]. In general, forward pumped DRA produces lower ASE noise and less double-Rayleigh scattering [5] in comparison to backward pumping. However, the effects of pump intensity noise on the optical signal are more pronounced for forward pumping [5], [6] primarily due to the slow walk-off between the pump and the signal. As the next generation unrepeatered systems are required to transport high volume traffic for longer reach, migrating from QPSK to 16-QAM and 64-QAM is a preferred solution to increase the capacity. However, higher order modulation formats are less resilient to RPN and may not favor the use of forward pumping, resulting in a capacity-reach tradeoff. Aside from pump RIN effects, forward pumping amplifies the signal power at the beginning of the fiber span which could trigger fiber nonlinear effects. Most of the reported experimental demonstrations of unrepeatered transmissions made use of single carriers with QPSK modulation and high baud rates (28$\sim$32 Gbaud, including FEC overhead) [7], [8]. In such systems, RPN may not be the most significant impairment to the information signal, and any Kerr effect induced nonlinearities can be compensated using digital backpropagation (DBP) as reported in [11].

Despite the fact that most of the current deployed systems are based on single carrier per wavelength, interest in digital subcarrier multiplexed transmission technology (DSCM) has been increasing from both academic research and commercial standpoint. In a DSCM system, the desired net baud rate is achieved by multiplexing multiple low baud rate subcarriers. The primary advantages of DSCM from a system's perspective are: enhanced tolerance to both fiber nonlinearity and equalization enhanced phase noise, and flexible spectral efficiency by modulating individual subcarriers with different modulation formats and bandwidths [12]. We can reap the complete benefits of DSCM by optimizing the baud rates of individual subcarriers which is in the order of 2$\sim$6 G Baud for the present systems [13], [14]. It has been recently reported that, for high net baud rate systems operating beyond 32 Gbaud, DSCM offers increased reach compared to a single carrier transmission [14]. Therefore, DSCM could be a viable solution to realize a high capacity transmission system especially over long span repeaterless links.

The downside of DSCM systems with higher order modulation formats is its limited tolerance to phase noise compared to single carrier systems for a given linewidth of the laser source. This is attributed to linewidth-symbol-time product that has to be below a certain value so that the digital phase noise compensation algorithms can track and compensate the phase noise. With modern external cavity lasers offering low linewidths [$\sim$ $<$100 kHz], the difference in the phase noise performance between single carrier and DSCM systems can be minimized by joint processing, i.e., averaging the estimated phase noise from all the subcarriers and using this averaged phase estimate to correct the phase noise [12]. Note that, joint processing was proposed to avoid differential encoding/decoding overhead. This averaging technique for DSCM has been validated experimentally for QPSK using Viterbi-Viterbi phase correction [15]. As averaging minimizes the impact of ASE noise and the probability of slips on the estimated phase, it has to be performed before unwrapping the phase estimate, as averaging after unwrapping will not compensate phase slips [16]. For higher order QAM modulation formats, blind phase search (BPS) algorithm for tracking phase noise offers best performance at the cost of complexity. However, averaging the estimates of individual subcarriers' phase noise is possible only after unwrapping the phase. Therefore, the possibility of phase

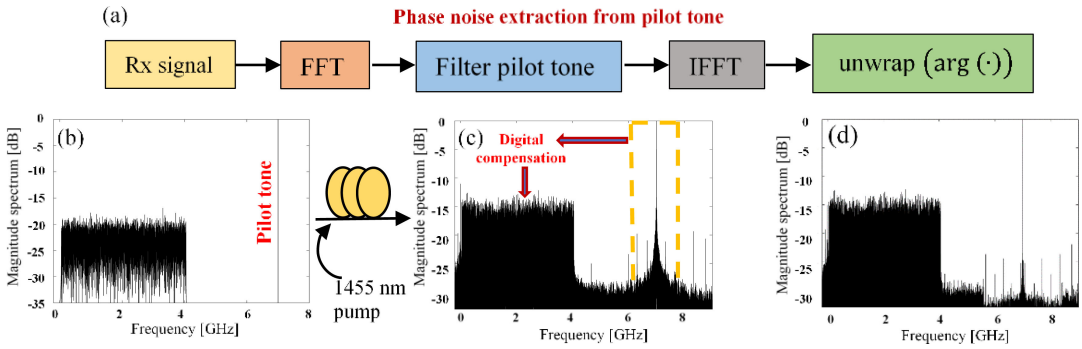

Fig. 1. (a) Procedure for extracting phase noise information from pilot tone {(I)FFT): (Inverse)Fast Fourier Transform, arg: argument of the complex signal}; Magnitude spectrum of (b) transmitted signal, (c) received signal, and (d) RPN compensated signal.

slips in the unwrapped phase estimates renders simple phase averaging ineffective. In [17], the authors propose a method for compensating these phase slips by comparing the phase estimates of a particular subcarrier with the average of all other subcarriers. The performance enhancements are promising for reasonably small linewidth symbol time products (1×10^{-4}). However, in the context of forward pumped DRAs using high power pump lasers with inherently high levels of RIN, joint processing of subcarriers may not be a feasible solution to mitigate RPN. This is because high phase noise content results in signal subcarriers to have phase slips at either same time instant and /or multiple phase slips at different time instants.

In this paper, we present the first proof-of-concept demonstration of a simple pilot aided RPN compensation for a coherent fiber-optic system using 16-QAM modulation format and DRA with forward pumping. The proposed technique achieves significant improvement in BER performance compared to conventional blind phase search compensation, especially for low baud rate signals. Using the measured pump intensity waveform together with numerical simulation, we demonstrate the proposed technique in the context of DSCM transmission with 2.5 Gbaud and 5 Gbaud subcarriers for an aggregated symbol rate of 25 Gbaud. Together with backward pumping and ROPA, we expect that the proposed RPN compensation technique can extend the reach of high capacity unrepeatered transmission system using higher order QAM modulation formats and subcarrier multiplexing.

2. Principle of Pilot Aided RPN Compensation

The implementation of pilot aided RPN compensation adds a pilot tone to the information signal in the transmitter, with a finite spectral gap between them. This pilot tone can be introduced in three different ways: (i) digitally (digital pilot tone) (ii) in analog electronic domain using an off-the-shelf RF signal generator and (iii) in optical domain using the transmit laser itself by biasing the optical IQ modulation slightly away from the transmission null point. When both information signal and pilot tone are modulated onto the optical field of the same CW laser and transmitted along the fiber system with DRA, RPN will have nearly identical impact on the signal and the pilot. Therefore, at the receiver, after coherent detection and digitizing, pilot tone can be selected through a digital filter to extract its RPN as a function of time. This waveform can then be used to eliminate the effects of RPN on the received information signal. A block diagram illustrating this process is shown in Fig. 1(a). Figs. 1(b) through 1(d) show the spectra of the transmitted, received and RPN compensated signals, clearly depicting the effects of RPN and its compensation. Mathematically, let $E(t)$ be the complex field of the received electric signal, which is linearly proportional to the complex field of the optical signal in a coherent detection receiver. $E(t)$ consists of information signal $s(t)$ and pilot tone $p(t)$, i.e., $E(t) = (s(t) + p(t))\, e^{j\phi(t)}$, where, $\phi(t)$ is the RPN transferred from the pump

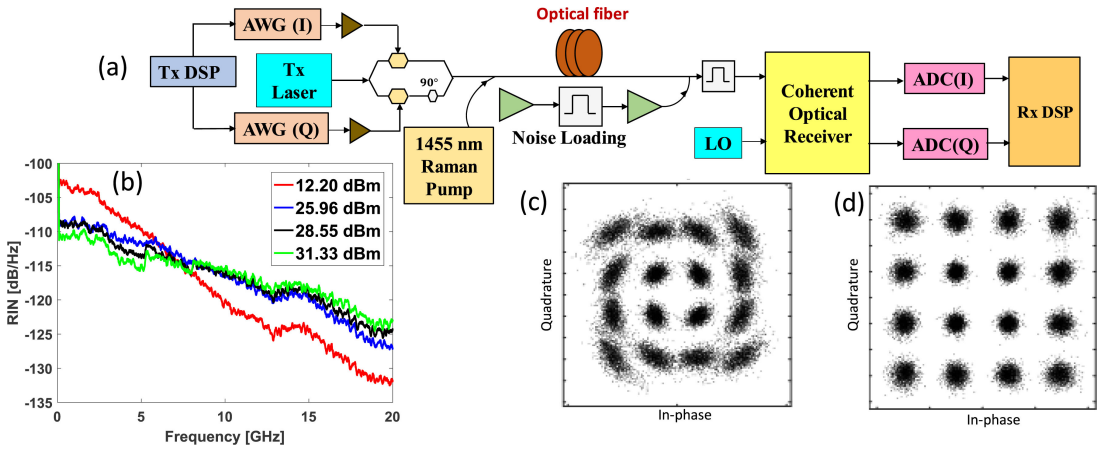

Fig. 2. (a) Experimental setup block diagram, (b) Measured RIN spectra for different pump powers; Constellation diagrams (c) without and (d) with pilot aided RPN compensation.

intensity to signal phase due to XPM. Let $\hat{\phi}(t)$ be the estimated phase noise from the pilot tone selected with a digital filter. In pilot aided RPN compensation, $E(t)$ is re-modulated with inverse of the estimated phase noise, i.e., with $e^{-j\,\hat{\phi}(t)}$. This results in

$$\hat{E}(t) = E\,(t)\;\; e^{-j\,\hat{\phi}(t)} = (s(t) + p\,(t))\;\; e^{j\left(\phi(t) - \hat{\phi}(t)\right)} \tag{1}$$

Ideally, in a high OSNR regime with strong pilot tone and a wide bandwidth digital filter to select the pilot, $\hat{\phi}(t) = \phi(t)$, so that the effect of RPN on the information signal can be completely removed. However, in a practical system with ASE noise, the compensation may not be complete; the power ratio between the pilot tone and the information signal, as well as the digital filter bandwidth have to be optimized according to both OSNR and RPN of the system. In general, XPM efficiency between optical channels is dependent on their frequency separation [18]. In silica-based optical fiber, the Raman shift is on the order of 13 THz between the pump and the information signal, while the frequency difference between the pilot tone and the information signal is only a few GHz, and thus, the XPM efficiency difference between pilot and information signal is negligible. This allows the phase noise information on pilot to be used to compensate the same on the information signal. In practical implementations of DRA, pump modules with multiple pump lasers (wavelength multiplexed) or higher order cascaded pump sources are widely adopted. In such a scenario, it is interesting to note that the pilot tone captures the combined RPN arising from RIN of all the pump sources, thereby allowing the digital receiver to compensate the effective RPN. In fact, the use of pilot tones has also been demonstrated to compensate signal induced XPM [19] and laser phase noise [20] in coherent optical systems.

3. Experimental Setup, Results and Discussion

The Experimental setup is shown in Fig. 2(a). A Nyquist pulse shaped (with roll-off factor of 0.001) 4.2 Gbaud 16-QAM signal along with a pilot tone is digitally generated offline. Fig 1(b) shows the baseband electrical spectrum of the transmitted signal in which the pilot tone is positioned at 7 GHz. In-phase (I) and quadrature (Q) components of the signal are loaded into the memory of an arbitrary waveform generator (AWG) operating at approximately 22 GSamp/s. The two analog outputs are amplified to drive an IQ electro-optic modulator. The IQ modulator is biased for complete optical carrier suppression and optical single sideband (OSSB) modulation. An external cavity laser (ECL) with 100 kHz spectral linewidth is used as both the light source in the transmitter and as the local oscillator (LO) in the coherent receiver for complex optical field detection. The modulated signal is combined with the Raman pump through a 1450/1550 nm WDM coupler and launched into a 73 km

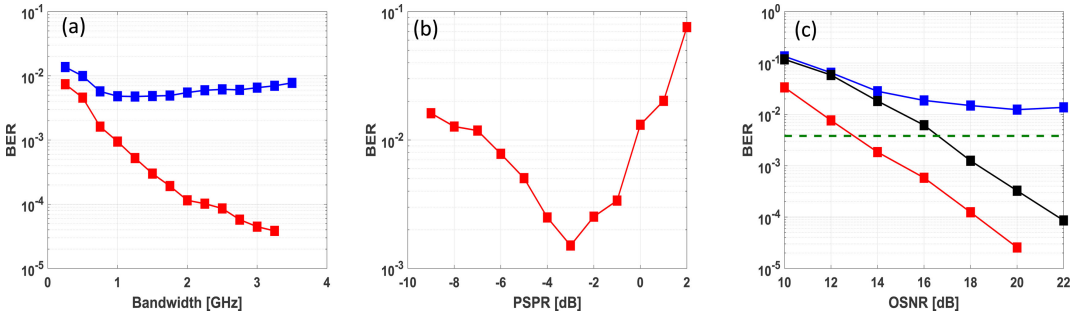

Fig. 3. (a) Optimization of pilot filter bandwidth at OSNR of 16 dB (blue) and 22 dB (red), (b) Plot of BER versus PSPR, (c) Plot of BER as a function of OSNR: blue: forward pumping, without pilot aided RPN compensation; black: forward pumping, with pilot aided RPN compensation; red: backward-only pumping, green: HD-FEC threshold (BER $= 3.8 \times 10^{-3}$).

standard single mode fiber (SSMF). The pump laser used in this work is a cladding pumped fiber laser based on cascaded Raman resonators emitting at 1455 nm wavelength. While this pump laser can offer high power of up to 10 W, its RIN is also high, on the level of $-100 \sim -110$ dB/Hz in the low frequency region. The measured RIN spectra are shown in Fig. 2(b) for different pump powers. In the present experiment, pump power of approximately 26.8 dBm (corresponding to 1.35A drive current) was launched into the SSMF yielding 12 dB Raman on-off gain. At the fiber output, signal is loaded with ASE noise generated from a pair of EDFAs followed by tunable optical bandpass filters of 1 nm bandwidth. The optical signal power at the input of the coherent receiver is -18 dBm, and the LO power is approximately 10 dBm. After coherent reception, the I and Q components of the photocurrents are captured and digitized using a real time digital oscilloscope. The received data is processed offline. As a part of receiver DSP, firstly, fiber dispersion is compensated to align the phases of pilot and the signal. Next, pilot tone is shifted to the baseband to extract its phase noise through a lowpass boxcar digital filter with 2.5 GHz bandwidth. After pilot aided RPN compensation, the signal is normalized and synchronously down-sampled to 2 samples per symbol, followed by a 19 tap T/2 spaced adaptive digital filter that compensates IQ skew and residual timing offsets [21]. In the absence of pilot aided RPN compensation, blind phase search with 64 test phases averaged over 19 symbols is used to track RPN [22]. This is followed by maximum likelihood symbol decision making and BER estimation. BER was measured over 261120 bits. For this demonstration, we used differential encoding/decoding of QAM symbols to tackle cycle slip induced error bursts in the case of blind phase search compensation. Fig. 2(c) and 2(d) show examples of constellation diagrams without and with pilot aided RPN compensation, respectively.

Reserving a sufficient spectral gap between information signal and pilot tone enabled us to study the impact of digital filter bandwidth for extracting the phase noise from the pilot. When operating in high OSNR regime with sufficient pilot power relative to signal power (i.e., when system performance is limited by RPN), a large pilot filter bandwidth can capture high frequency components of the phase noise and effectively compensate its impact on the information signal. However, in the presence of ASE noise, a large pilot filter bandwidth can be more susceptible to the impact of ASE noise, which deteriorates the effectiveness of pilot aided RPN compensation. Fig. 3(a) demonstrates the impact of pilot filter bandwidth on the BER with OSNR levels of 16 dB and 22 dB, respectively (at 0.1 nm resolution bandwidth). For 16 dB OSNR, a global minimum of BER was found at the filter bandwidth of approximately 1 GHz. However, for 22 dB OSNR, BER monotonically decreases with increasing the filter bandwidth. Another important parameter to be optimized is the pilot-to-signal power ratio (PSPR). For systems with low PSPR, in the presence of ASE noise, the pilot tone does not have high enough SNR to accurately capture the RPN. On the other hand, if the PSPR is too high, the signal optical power could be significantly depleted by the pilot, and the system can become ASE noise limited. Therefore, joint optimization of PSPR and pilot filter bandwidth is necessary to obtain best possible results for a given system OSNR. For the system under consideration, the impact of

PSPR on BER for an OSNR of 17 dB and with a 2.5 GHz fixed pilot filter bandwidth is shown in Fig 3(b). Apparently, there is an optimum PSPR that minimizes BER for a given OSNR. Based on this result, we used a PSPR of -3 dB for BER measurements across all OSNRs, and results are shown in Fig. 3(c). Note that a pilot tone with -3 dB PSPR is equivalent to a 1.76 dB signal power penalty. Without pilot aided RPN compensation, i.e., when only blind phase noise compensation is used to compensate RPN, an error floor is reached at a BER level of approximately 10^{-2}, which is above the HD-FEC threshold of 3.8×10^{-3}. It is evident that pilot aided RPN compensation yields a significant improvement in BER performance by eliminating this BER floor. As a reference, BER curve with backward-only pumping DRA at the same Raman gain is also shown in the Fig. 3(c). Comparing the three curves in Fig. 3, we can clearly see the detrimental effect of pump RIN induced RPN on the signal when forward pump is used. Note that, when computing OSNR at the receiver side, the noise power has contributions from both ASE noise that is loaded as well as ASE noise generated by spontaneous Raman scattering. Therefore, for the same Raman on-off gain, the actual loaded noise power is slightly high for forward pumping than backward pumping. Despite the fact that the same differential encoded data has been used to obtain BER plots corresponding to with and without pilot aided RPN compensation (Fig. 3(c)), real systems using pilot aided RPN compensation do not need to use differential encoding. This allows the use of conventional SD-FEC schemes without any iterative turbo demodulation [23], [24], reducing the feedback latency between FEC and differential decoder. Additionally computational complexity for extracting the pilot tone in terms of the number of complex multipliers is given by $(2 \times \frac{N}{2}\, log_2\,(N)) + (N)$, where N is the number of samples.

4. Simulation of a 25 Gbaud DSCM Transmission Using Measured Pump RIN Waveforms

Due to the transmitter bandwidth limitation, only 4.2 Gbaud signal was used in the transmission experiment reported in Section 3. In this section we show the feasibility of pilot aided RPN compensation for more generalized DSCM systems at higher baud-rates using numerical simulations but based on measured pump RIN waveforms. To simulate the effect of RIN transfer from pump to signal, we numerically solve the nonlinear Schrödinger equations (NLSE) (2) and (3), which govern the propagation of pump and signal optical fields, A_p (t) and A_s (t), along the fiber

$$\frac{\partial A_p}{\partial z} = -\frac{\alpha_{\text{pump}}}{2} A_p + i\gamma_{\text{pump}} |A_p|^2 A_p \tag{2}$$

$$\frac{\partial A_s}{\partial z} = d\frac{\partial A_s}{\partial T} - \frac{\alpha_{\text{signal}}}{2} A_s + i\gamma_{\text{signal}} (2 - f_R) |A_p|^2 A_s + \frac{g_s}{2} |A_p|^2 A_s \tag{3}$$

For the present discussion, the signal optical field A_s (t), represents a DSCM signal together with the pilot tone which is generated using MATLAB. Instead of numerically generating the pump optical field, A_p(t), we experimentally measure and capture the pump laser's RIN waveform, and use this waveform to represent A_p (t). By incorporating the actual pump laser's intensity noise waveform in the numerical simulation, the observed impact of RPN on the information signal is realistic and close to the real transmission experiments. Fig 4(a) shows the experimental setup to measure the pump laser's RIN. Pump laser's output is connected to an optical attenuator before been detected with a photodetector. The photocurrent is sampled, recorded for a duration of 20 μs at a sampling frequency of 50 Gsps using a real time digital oscilloscope and processed offline in MATLAB. The measured intensity noise waveform is normalized by the optical power to obtain the RIN and calibrated to account for the photodetector responsivity. Fig. 4(b) shows the numerical simulation setup which involves generation of DSCM signal along with pilot tone, propagation of pump and signal waveforms through the fiber using (2) and (3) and finally applying DSP techniques on the output signal after fiber transmission.

Signal waveform A_s(t) is composed of five 5 Gbaud Nyquist spectral shaped subcarriers (roll-off factor of 0.001) with differentially encoded 16-QAM symbols. This corresponds to a net symbol

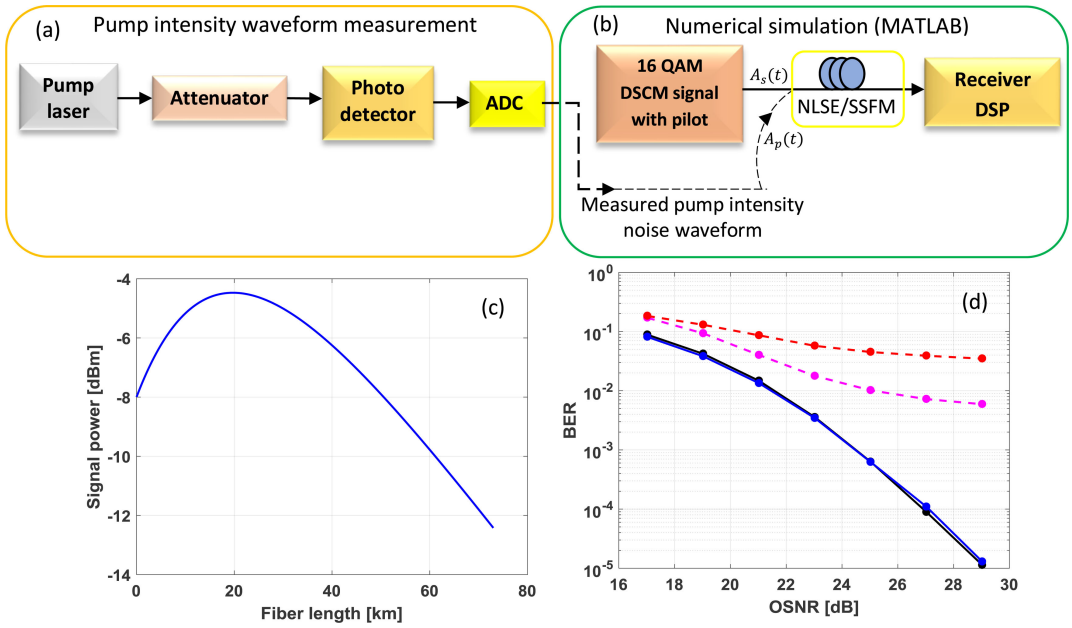

Fig. 4. (a) Experimental setup for measuring intensity noise of pump, (b) Numerical simulation setup for DSCM transmission (c) Signal power evolution along the simulated fiber, (d) BER curves as a function of OSNR. Red: 2.5 Gbaud subcarrier, without pilot aided compensation, magenta: 5G baud subcarrier, without pilot aided compensation, blue: 2.5 Gbaud subcarrier with pilot aided compensation, black: 5 Gbaud subcarrier with aided pilot compensation.

rate of 25 Gbaud, equivalent to a 200 Gb/s data rate (excluding FEC overhead) if polarization-multiplexing is used. The pilot tone is positioned on one side of the signal spectrum, with a PSPR of -6 dB, which is optimized for OSNR of 23 dB. Throughout the simulation, we assume the use of transmit laser and local oscillator laser with zero linewidth, an ideal DAC, ideal optical IQ modulator with linear driving amplifiers, and an ideal ADC. Note that, in real transmission systems, to generate an optical single sideband DSCM signal, the in-phase and quadrature components of the desired waveform can be obtained using similar technique as described in [26]. The signal and calibrated pump waveforms are propagated through the non-linear equations (2) and (3) for 73 km SSMF, using split-step Fourier method (SSFM) with uniform step size of 10 m. The numerical values of various parameters used in Eqn (2) and (3) are given as: pump and signal attenuation coefficients $\alpha_{pump} = 0.24\ dB/km$, and $\alpha_{signal} = 0.22$ dB/km; nonlinear coefficient at the pump and the signal wavelengths $\gamma_{pump} = 1.3\ \mathrm{W}^{-1}\ \mathrm{km}^{-1}$ $\gamma_{signal} = 1.2\ \mathrm{W}^{-1}\ \mathrm{km}^{-1}$, walk off parameter $d = 1.6$ ps/m, and Raman gain coefficient $g_s = 0.33\ \mathrm{W}^{-1}\ \mathrm{km}^{-1}$. The evolution of the signal power along the fiber length is shown in Fig. 4(c). After the simulation of nonlinear propagation, additive white Gaussian noise is used to simulate the effect of ASE noise loading. Post fiber transmission, the signal is processed using similar DSP as applied on the experimental data in Section 3. In particular, signal is dispersion compensated, followed by pilot aided relative phase noise compensation. The desired subcarrier is frequency translated to the baseband, filtered using a matched Nyquist filter and adaptively equalized before performing decision making, differential decoding, and error counting. In the absence of pilot aided RPN compensation, blind phase search with 64 test phases, averages across 19 symbols is used to track RPN. Fig. 4(d) shows the BER versus OSNR (0.1 nm resolution bandwidth) curves for the central subcarrier, both with and without pilot aided RPN compensation. The plot also shows the BER curves for the same total baud rate but with ten 2.5 Gbaud subcarriers. The performance degradation due to RPN is more severe for 2.5 Gbaud subcarriers than 5 Gbaud subcarriers because of the lower symbol time-linewidth product. Although numerical simulation usually predicts better performance compared to actual transmission experiments due to the assumed

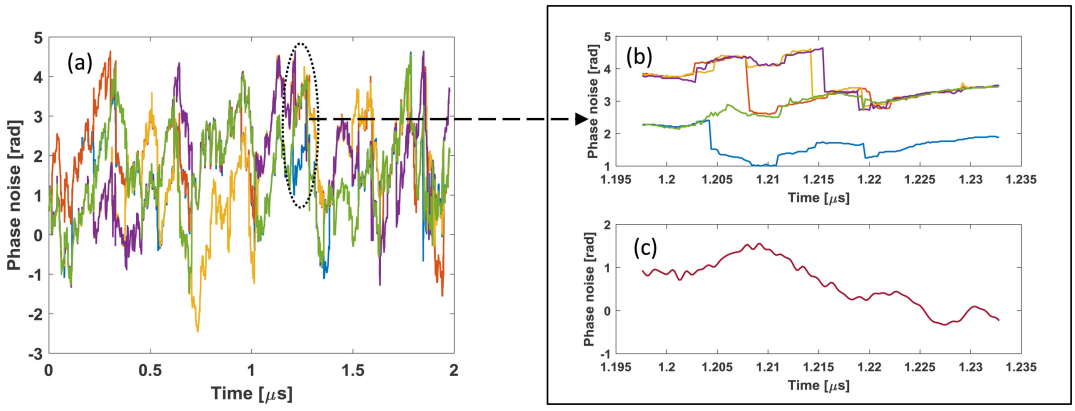

Fig. 5. (a) and (b) Plot of unwrapped phase noise estimates using blind phase search for all the five 5 Gbaud subcarriers, superimposed; 5(c) phase noise estimate obtained from filtered pilot tone.

ideal nature of certain optical and electronic components, it helps better understand mechanisms of performance degradation. It is important to note that propagation equations (2) and (3) do not consider the ASE noise generation by spontaneous Raman scattering, so the nonlinear interaction between signal and noise in the fiber is neglected. In the above simulation, the spectral overhead due to the pilot tone is about 10% (2.5 GHz pilot bandwidth vs. 25 GHz signal bandwidth), and in general the spectral overhead due to the pilot tone can be further decreased by increasing the net baud rate of the system.

Finally, to test the feasibility of joint processing of subcarriers by averaging their phase noise estimates, Fig. 5 shows the RPN phase noise traces estimated using blind phase search with phase unwrapping for all the five 5Gbaud subcarriers. We can clearly see multiple phase jump events in a time span of just 2 μs corresponding to 10000 symbols. Fig. 5(b) zooms into a short time span of Fig. 5(a) with more details, which clearly shows multiple phase slip occurrences. For comparison, Fig. 5(c) shows the phase noise estimated from the filtered pilot tone, which clearly maintains the phase continuity. This result indicates that joint processing of multiple subcarrier channels may fail when the effect of RPN is sufficiently high, and in comparison, pilot-aided compensation is much more robust in avoiding phase slips as shown in Fig. 5(c).

5. Conclusion

In conclusion, we have experimentally demonstrated an efficient pilot-aided digital compensation of RPN, in a distributed Raman amplified coherent transmission system involving forward pumping. We show that the high RIN from a high power Raman laser can produce significant RPN in the phase modulated optical signal which often results in BER floor, especially when relatively low baud rates are used as in DSCM transmission systems. Pilot-aided digital compensation with adequate pilot filter bandwidth and PSPR can help eliminate the error floor. As an extension of the experimental results, we inserted the measured pump laser RIN into numerical simulations to further demonstrate the effectiveness of pilot aided compensation in the context of DSCM system using 16-QAM, with five and ten subcarriers for a net symbol rate of 25 Gbaud.

References

[1] J. Renaudier, R. Rios-Müller, P. Tran, L. Schmalen, and G. Charlet, "Spectrally efficient 1-Tb/s transceivers for long-haul optical systems," *J. Lightw. Technol.*, vol. 33, no. 7, pp. 1452–1458, Apr. 1, 2015.

[2] J. Cho *et al.*, "Trans-atlantic field trial using probabilistically shaped 64-QAM at high spectral efficiencies and single-carrier real-time 250-Gb/s 16-QAM," in *Proc. Opt. Fiber Commun. Conf. Exhib.*, Los Angeles, CA, USA, 2017, pp. 1–3.

[3] J. Cai *et al.*, "49.3 Tb/s transmission over 9100 km using C+L EDFA and 54 Tb/s transmission over 9150 km using hybrid-raman EDFA," *J. Lightw. Technol.*, vol. 33, no. 13, pp. 2724–2734, Jul. 1, 2015.
[4] A. Ghazisaeidi *et al.*, "Advanced C+L-band transoceanic transmission systems based on probabilistically shaped PDM-64QAM," *J. Lightw. Technol.*, vol. 35, no. 7, pp. 1291–1299, Apr. 1, 2017.
[5] W. S. Pelouch, "Raman amplification: An enabling technology for long-haul coherent transmission systems," *J. Lightw. Technol.*, vol. 34, no. 1, pp. 6–19, Jan. 1, 2016.
[6] J. Bromage, "Raman amplification for fiber communications systems," *J. Lightw. Technol.*, vol. 22, no. 1, pp. 79–93, Jan. 2004.
[7] D. Chang *et al.*, "Unrepeatered 100G transmission over 520.6 km of G.652 fiber and 556.7 km of G.654 fiber with commercial Raman DWDM system and enhanced ROPA," *J. Lightw. Technol.*, vol. 33, no. 3, pp. 631–638, Feb. 1, 2015.
[8] D.-I. Chang, P. Patki, S. Burtsev, and W. Pelouch, "8 $\times$ 120 Gb/s transmission over 80.8 dB / 480.4 km unrepeatered span," in *Proc. Opt. Fiber Commun. Conf. Expo./Nat. Fiber Opt. Eng. Conf.*, Anaheim, CA, USA, 2013, pp. 1–3.
[9] L. Xu *et al.*, "Experimental verification of relative phase noise in raman amplified coherent optical communication system," *J. Lightw. Technol.*, vol. 34, no. 16, pp. 3711–3716, Aug. 15, 2016.
[10] C. Martinelli, L. Lorcy, A. Durecu-Legrand, D. Mongardien, and S. Borne, "Influence of polarization on pump-signal RIN transfer and cross-phase modulation in copumped raman amplifiers," *J. Lightw. Technol.*, vol. 24, no. 9, pp. 3490–3505, Sep. 2006.
[11] G. Saavedra, D. Semrau, L. Galdino, R. I. Killey, and P. Bayvel, "Digital back-propagation for nonlinearity mitigation in distributed Raman amplified links," *Opt. Exp.*, vol. 25, pp. 5431–5439, 2017.
[12] D. Krause, A. Awadalla, A. S. Karar, H. Sun, and K. Wu, "Design considerations for a digital subcarrier coherent optical modem," in *Proc. Opt. Fiber Commun. Conf. Exhib.*, Los Angeles, CA, USA, 2017, pp. 1–3.
[13] K. Kojima, T. Yoshida, K. Parsons, T. Koike-Akino, D. S. Millar, and K. Matsuda, "Comparison of nonlinearity tolerance of modulation formats for subcarrier modulation," in *Proc. Opt. Fiber Commun. Conf.*, 2018, paper M2C.4.
[14] O. Vassilieva, I. Kim, and T. Ikeuchi, "Enabling technologies for fiber nonlinearity mitigation in high capacity transmission systems," *J. Lightw. Technol.*, to be published, doi: 10.1109/JLT.2018.2877310.
[15] S. M. Bilal, C. Fludger, and G. Bosco, "Carrier phase estimation in multi-subcarrier coherent optical systems," *IEEE Photon. Technol. Lett.*, vol. 28, no. 19, pp. 2090–2093, Oct. 1, 2016.
[16] M. G. Taylor, "Phase estimation methods for optical coherent detection using digital signal processing," *J. Lightw. Technol.*, vol. 27, no. 7, pp. 901–914, Apr. 1, 2009.
[17] M. Qiu, Q. Zhuge, M. Chagnon, F. Zhang, and D. V. Plant, "Laser phase noise effects and joint carrier phase recovery in coherent optical transmissions with digital subcarrier multiplexing," *IEEE Photon. J.*, vol. 9, no. 1, Feb. 2017, Art no. 7901013.
[18] R. Hui, K. R. Demarest, and C. T. Allen, "Cross-phase modulation in multispan WDM optical fiber systems," *J. Lightw. Technol.*, vol. 17, no. 6, pp. 1018–1026, Jun. 1999.
[19] L. B. Y. Du and A. J. Lowery, "Pilot-based XPM nonlinearity compensator for CO-OFDM systems," *Opt. Exp.*, vol. 19, pp. B862–B867, 2011.
[20] G. Vedala, M. O' Sullivan, and R. Hui, "Digital phase noise compensation for DSCM-based superchannel transmission system with quantum dot passive mode-locked laser," *IEEE Photon. J.*, vol. 10, no. 4, Aug. 2018, Art no. 7202811.
[21] R. Rios-Müller, J. Renaudier, and G. Charlet, "Blind receiver skew compensation and estimation for long-haul non-dispersion managed systems using adaptive equalizer," *J. Lightw. Technol.*, vol. 33, no. 7, pp. 1315–1318, Apr. 1, 2015.
[22] T. Pfau, S. Hoffmann, and R. Noé, "Hardware-efficient coherent digital receiver concept with feedforward carrier recovery for *M*-QAM constellations," *J. Lightw. Technol.* vol. 27, no. 8, pp. 989–999, Apr. 2009.
[23] F. Yu *et al.*, "Soft-decision LDPC turbo decoding for DQPSK modulation in coherent optical receivers," in *Proc. 37th Eur. Conf. Expo. Opt. Commun.*, 2011, paper We.10.P1.70.
[24] T. Koike-Akino *et al.*, "Cycle slip-mitigating turbo demodulation in LDPC-coded coherent optical communications," in *Proc. Opt. Fiber Commun. Conf.*, San Francisco, CA, USA, 2014, pp. 1–3.
[25] G. P. Agrawal, *Nonlinear Fiber Optics*, 5th ed. New York, NY, USA: Academic, 2013, pp. 295–352.
[26] Y. Zhang, M. O'Sullivan, and R. Hui, "Digital subcarrier multiplexing for flexible spectral allocation in optical transport network," *Opt. Exp.*, vol. 19, no. 22, pp. 21880–21889, 2011.